Grain boundary strain as a determinant of localized sink efficiency

James E. Nathaniel II[a,b,1], Pranav K. Suri[b,1,2], Emily M. Hopkins[a], Jianguo Wen[c], Peter Baldo[c], Marquis Kirk[c], Mitra L. Taheri[a,*]

[a] Department of Materials Science & Engineering, Johns Hopkins University, Baltimore, MD, USA
[b] Department of Materials Science & Engineering, Drexel University, Philadelphia, PA, USA
[c] Center for Nanoscale Materials, Argonne National Laboratory, Lemont, IL, 60439, USA

A R T I C L E I N F O

Article history:
Received 30 July 2021
Revised 27 December 2021
Accepted 3 January 2022
Available online 8 January 2022

Keywords:
Sink efficiency
Grain boundary
Ion irradiation
Elastic strain

A B S T R A C T

The opportunity to achieve radiation tolerance in crystalline materials hinges on understanding the structure and response of grain boundary sinks to irradiation. A common descriptor of grain boundary efficiency as a defect sink is the denuded zone, which is a defect free zone adjacent to the grain boundary dictated by its ability to absorb radiation induced defects. This descriptor is often used at the mesoscale, which requires an averaging of absorption events. In this paper, we resolve the defect sink efficiency as a function of interfacial strain with respect to grain boundary character, and correlate high levels of grain boundary strain to an enhanced absorption efficiency. We also introduce a key relationship between localized strain in proximity with the grain boundary sink and the variation absorption efficiency associated with these regions, revealing the pitfalls of averaging absorption events along a grain boundary, and presenting a path forward toward improved models for denuded zones and localized grain boundary absorption phenomena.

1. Introduction

In recent years, much attention has been put toward the development of advanced materials possessing, enhanced radiation tolerance and the capacity to heal damage, thereby markedly improving the safety and sustainability of nuclear energy. One strategy to reducing or removing radiation-induced damage is grain boundary (GB) engineering, an approach in which materials are processed to obtain microstructures with specific GB character distributions. GBs act as sinks for radiation induced defects where the defects are absorbed and effectively eliminated [1–3]; however, numerous studies have demonstrated wide variations in sink behavior of different interfaces [4–7].

GB sink efficiency, η, is a parameter that characterizes the ability of GBs to absorb nearby point defects and is defined as the ratio of defects absorbed by a particular boundary to defects absorbed by a perfect boundary in which defects are not reemitted, $\eta = J_{measure}/J_{perfect}$ [4,8–11]. Sink efficiency can be explicitly quantified through the characterization of point defect concentration near the GB [12]. It is also known to be a function of the degrees of freedom of a GB, both macroscopic (including misorientation angle and the GB plane) and microscopic, yet direct measurements of GB character dependencies are not straightforward [13]. Currently, the most widely utilized experimentally quantifiable indicator of defect sink efficiency, has been the width of defect free areas adjacent to interfaces known as defect denuded zones [9,14]. The correlation between GB sink efficiency and defect denuded zone formation near the grain boundary can be quantified through the relationship between the efficiency, η, to denuded zone width, $\lambda_{D,Z}$, as illustrated in Beyerlein et al. [15]:

$$\lambda_{i,v}\sqrt{\frac{k_{sv,i}}{D_{v,i}}} = \ln \eta_{i,v} - \ln\left(1 - \Delta c_{v,i}\frac{k_{sv,i}}{k_0}\right), \tag{1}$$

where $\lambda_{i,v}$ is the denuded zone width, $k_{sv,I}$ is the coefficient of the defect-sink reaction rate, k_0 is the defect diffusivity within the grain, Δc is the critical defect concentration for loop or void nucleation. In Eq. (1), η represents the sink efficiency describing the capability of the sink to absorb defect clusters as a GB is evolving with point defect insertion; i and v indicating interstitial and vacancy, respectively. In the present study, the ability of the individual GBs to absorb defects, hereinafter is designated as “sink efficiency (η)”. Denuded zones are consequential side effects of defect interactions with sinks. Experiments in Cu [16], Au [17], and NiCr [18] have all shown that the denuded zone widths in materials may vary significantly with GB character. Han et al. investi-

* Corresponding author, 410-516-5592, Maryland Hall 207, Johns Hopkins University, Baltimore, MD 21218.
E-mail address: mtaheri4@jhu.edu (M.L. Taheri).

[1] These authors contributed equally to this work.
[2] Current address: Micron Technology, Inc., Boise, ID, USA

gated the GB character dependence of void denuded zones (VDZs) in Cu foils irradiated with He ions using transmission electron microscopy (TEM) and electron backscatter diffraction (EBSD); variations in the widths of the VDZs as well as the size and density of voids showed strong dependence on GB misorientation angles and GB plane normals [9,19]. For $\Sigma3<110>$ tilt GBs, the VDZ width increased with increasing GB plane inclination angle and VDZ widths at non-$\Sigma3$ GBs were larger than at $\Sigma3<110>$ tilt GBs. According to Tschopp and McDowell [20], increasing the inclination angle for $\Sigma3$ tilt GBs results in an increase in symmetric incoherent twin boundary structural units, which in turn leads to more trapping sites for point defects, which deplete the vacancy concentration near the GBs.

Several studies have identified inconsistencies in the formation of defect denuded zones with respect to GB misorientation [21–23] as well as changes in sink behavior with changes with radiation conditions [24,25]. Contrary to Han's findings, in a similar study on He implanted nanocrystalline Fe thin films, El-Atwani et al. found that denuded zone formation had no correlation with misorientation angle [26]; however, their results indicated that denuded zone occurrence showed temperature dependence, and directionality of sink efficiency was observed in some asymmetric GBs [21]. Furthermore, theories suggesting that GB defect content can alter sink efficiency have been hypothesized but have yet to be experimentally validated due to technological limitations [27–31].

The efficiency of an interface in annihilating defects is characterized by its ability to readily absorb defects, which is one of the quintessential parameters in the rate theory models of radiation resistance [32–34]. The sink efficiency of a GB is dependent upon its structure and mechanisms of interaction with point defects; greater sink efficiency correlates with greater denuded zone width, thus, slowing defect accumulation around a GB under irradiation. Balluffi and Granato derived an expression for the sink strength of tilt GBs (a supposition which may be applicable for many grain boundary types) under diffusion-controlled conditions: assuming that point defects are trapped at the "hole" or jogs on edge misfit dislocations in the GBs, they conjectured that sink strength is inversely proportional to the average distance between point defect trapping sites within the boundary and the characteristic distance of diffusion of defects to the boundary [35,36]. Using molecular dynamics to investigate the mobility of defects at GBs by examining vacancy migration in $\Sigma5$ tilt boundaries, Balluffi et al.'s results yielded practical activation energies for migration and showed that the jump processes are highly structure dependent features of GB diffusion [37,38]. By calculating the kinetic properties of point defects at special boundaries, Sørensen et al. recognized that GB structure also determines whether vacancy or interstitial flux dominates GB interactions [39]. More recently, Frolov et al. established that the introduction of defects within GBs changes the boundaries' intrinsic structure and that "damaged boundaries" have significantly different properties than the initial pristine structures [29,30]. Complementary results from Uberuaga et al. revealed that damaged boundaries, modeled as GBs containing an excess of defects, have interactions with defects in the bulk of the material differing from pristine GBs [24,27]. These findings led to understanding that the sink efficiencies of the interfaces of materials under irradiation are dynamic and evolve with the defect concentration within the GBs and depend on both boundary character/structure and nonequilibrium conditions [31,40]. A complimenting contemporary study found that nonequilibrium GB states can provide preferential sites for stress propagation, and in turn, localized stress fields favor dislocation transmission sites [41]. Such localized stress fields are artifacts from inherent dislocations and point defects near the GB prior to defect absorption. Consequently, localized deviatoric stress is shown to be a dominating factor in elastic interactions between GBs and point defects through Monte Carlo simulation, enhancing interfacial sink strength through the reduction of defect migration barriers [38].

Molecular dynamics studies have also shown that GBs contain alternating regions of high tensile and compressive pressure that influence defect migration. Samaras et al. [42,43], mentioned that when the interstitial clusters approach interfaces within a few atomic layers, the clusters encounter the strong pressure gradients and preferentially migrate to regions under tensile stress along the GBs. The clusters continue to undergo 3D translations within the GB in order to maintain a migration path along low-pressure gradients until the defects are ultimately absorbed and settled into free volume in the GB structure, thereby relieving the tensile stain. Novel model conjectures help to frame the understanding of GB dynamics, yet further insight into the mechanisms and ramifications of defect absorption at GBs is in much need of experimental validation. Of particular interest are the implications of GB structure, strain, and defect concentration on sink efficiency: Are these parameters coupled or mutually exclusive? Do different interfaces reveal unique signatures? Does defect absorption exhibit a structure dependent codependence, and if so, how does the propensity for GBs to continue to absorb defects evolve with irradiation and at what scale, i.e. should sink efficiency be perceived as an aggregate or local descriptor?

While the influence of localized strain on defect absorption has been demonstrated, a reliance on averaging denuded zone absorption events to describe GB sink efficiency remains. High resolution techniques examining local regions of GB strain put forward more accurate descriptors of grain boundary absorption phenomena in real time. Several indirect methods have been applied to probe the structural state of GBs, including GB diffusion [44], GB mobility [45], and GB sliding resistance [46], however, confirmation of modifications by direct experimental observations is elusive due to the quantitative precision and instrumental resolution required to document atomic scale changes. In this regard, in situ and high-resolution transmission electron microscopy (HRTEM) have become influential tools for defect morphology inspection and interfacial strain mapping at the nanoscale made possible by the development of quantitative image analysis methods.

In this study, we connect local defect geometries and interfacial strain to defect absorption to uncover the sources of GB sink efficiency. Geometric phase analysis (GPA), a standard method for quantitative-relative strain analysis on the nanometer scale [47–52], is used to characterize variances in GB sink proficiency as a result of GB-defect interactions induced by heavy ion bombardment in Cu bicrystal samples. Inherent strain from localized dislocations in the interfacial structure of three distinct GBs was measured and correlated with defect absorption data contrived using a combination of in situ irradiation, HR-TEM techniques, and image processing. In calculating the defect cluster flux at different interfaces under the same experimental conditions, disparities in defect absorption rates amongst varying GB types imparts credence to the hypothesis that the observed diffusion behavior is consequence of distinct interface structural features which emanate elastic fields. Moreover, defect absorption rates corresponded with trends in relative strain measurements where, interestingly, the highest strain and fastest absorption rate belonged to the low angle GB (LAGB) 14º, followed by the high angle GB (HAGB) 22º with the median strain and absorption rates, and the coherent twin (CTB) $\Sigma3$ GB exhibiting the lowest strain and slowest, yet most consistent, absorption rate.

2. Experimental procedure

Bulk Cu bicrystals provided by collaborators at Los Alamos National Laboratory were wafered into 0.3 mm thick, 3.0 mm diameter discs via wire electrical discharge machining. The specimen wafers were then iteratively thinned by electrolytic polishing in a phosphoric acid solution until electron transparent areas approximately 20–40 nm thick were present. TEM characterization was used to inspect the samples and locate GBs within the thin regions. Initial TEM was done at Drexel University using a JEOL 2100F FEG; subsequent atomic resolution, energy-filtered imaging using the Argonne Chromatic Aberration-corrected (ACAT) FEI Titan 80–300 ST microscope with a CEOS Cc/Cs corrector was completed at Argonne National Laboratory. To avoid ambiguities and accentuate the impact of GB character, the three samples used contained GBs of different types exhibiting distinct misorientations angles: a 14° [10 -3 2] LAGB, a 22° [−9 −4 3] HAGB, and a Σ3 60° [−1 −1 1] CTB. GB angles were calculated by measuring the rotation angles between spots in Fourier transform filtered images and confirmed using automated crystal orientation mapping (ACOM). GB normal planes were determined to be {−1 −1 0}, {1 1 0}, and {1 1 1} for the LAGB, HAGB, and CTB, respectively given crystal coordinates and GB trace [53]. For detailed analysis, refer to the Supplementary Material (Figures S1-S3).

GPA [47,54,55] was performed on the atomic resolution TEM images to produce relative strain maps of the GBs before irradiation. Comprehensive relative strain analysis is based on lattice imaging taken with the aberration-corrected TEM to minimize imaging artifacts, e.g. delocalization of the image contrast at interfaces [56,57]. Initially proposed for the study of strained metal multilayers [58] and nanocrystals [59], GPA has been successfully applied to a wide variety of systems such as thin films [60], nanowires [61] and bilayer materials [62]; the accuracy of the technique has also been verified by the study of known dislocations in silicon [63,64]. GPA algorithms use Fast Fourier transforms of atomic resolution images to quantify displacement and strain fields in crystalline materials at nanoscale resolution. Strain in a region of interest (ROI) is measured relative to a reference area with minimal deformation within the sample. Fourier transforms of atomic resolution micrographs are used to obtain information about the lattice planes and calculate a geometrical phase image from which deformation maps are produced.

Irradiation experiments were conducted in situ at the IVEM at Argonne National Laboratory using the NEC implanter. Irradiation experiments were video recorded under a multibeam imaging condition to obtain sufficient image contrast and optimize defect observation. Samples were irradiated with 1 MeV $Kr^{2}+$ ions at room temperature under vacuum to a total damage level of 0.5 dpa (a fluence of $\sim 3.7 \times 10^{14}$ ions/cm^2). Damaged boundaries are expected to interact differently with defects than pristine boundaries, hence the low radiation dose was chosen to keep the GBs as pristine as possible while elucidating the initial stages of GB damage. The irradiation damage conditions were determined using the quick Kinchin-Pease calculation in SRIM 2013 with a 40 eV displacement threshold energy and 0 eV lattice binding energy for Cu. Nearly all incident Kr ions were expected to have been transmitted through the film without any implantation or backscattering. The SRIM simulation projected that the damage profile progresses linearly with the peak damage occurring beyond the foil thickness (see Fig. 1).

Quantitative characterization of the defect evolution was conducted by analyzing the in situ video frames post irradiation. Defect density was tracked with respect to damage dose/time in ROIs next to the GBs to calculate a defect absorption rate. Still frame images were extracted from the in situ videos in 60 second intervals corresponding to 0.01 dpa steps up to 0.1 dpa, then the sum of the projected areas of the visible defects in a 200 nm by 50 nm area adjacent to the GB (see Fig. 2a) was measured using the Photoshop selection tool and ImageJ particle analysis protocol as outlined in [65]. Defect densities were plotted as a function of dose/time, and defect absorption rates were calculated by measuring the initial

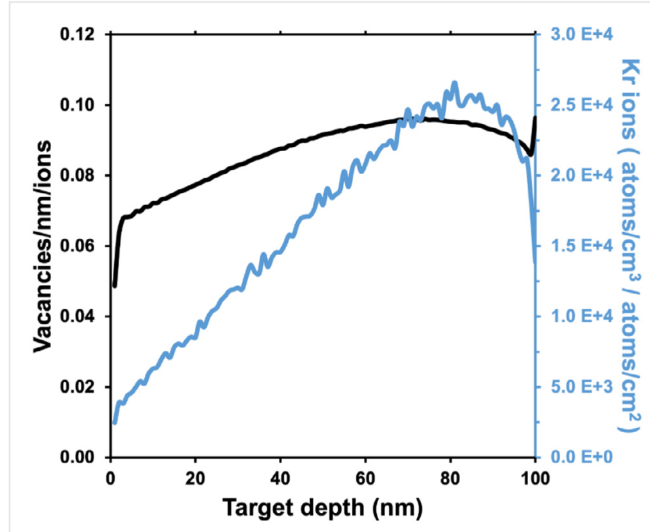

Fig. 1. SRIM results of Kr^{2+}ion bombardment of Cu: (black) the average damage per incident Kr ion per nm (damage profile) within the sample thickness and (blue) the penetration depth of ions.

slope of the linear fit of the defect density trend until the defect density values began to decrease.

Additionally, defect denuded zones were measured from micrographs collected of each of the three GBs studied at the terminal dose of 0.5 dpa. Denuded zone width was calculated by outlining and measuring the defect free area along 150 nm adjacent to the GBs using the freehand polygon tool in ImageJ then dividing by the length of the area (150 nm) (see Fig. 2b). For each GB the same analysis was performed on five images and then averaged.

3. Results

High-resolution micrographs of the three GBs of interest captured before irradiation are shown in Fig. 3: (Fig. 3a) low angle (LAGB) 14° [10 -3 2], (Fig. 3b) high angle (HAGB) 22° [−9 −4 3], and (Fig. 3c) a coherent twin (CTB) Σ3 60° [−1 −1 1]. GPA was performed on the micrographs to obtain deformation maps exhibited in Figs. 3d-f, respectively. Line scan strain profiles were acquired 1–2 nm adjacent to each GB as indicated by the dotted white rectangles on each respective deformation map. Relative strain measurements were normalized against a reference area selected in comparatively strain free areas away from the boundaries identified by the faint yellow squares annotated “ref”. The strain measure profiles for each GB are displayed in Figs. 3g-i, respectively, and the mean interfacial strain and standard deviation values are listed in Table 1. The LAGB had the highest interfacial strain at 0.71%, followed by the HAGB at 0.064%, and lastly the coherent Σ3 GB at −0.07%; positive strain values correlate to a tensile stress and negative values correlate to compressive.

Fig. 4 depicts the defect densities as a function of time (damage dose) up to 600 s (0.1 dpa) for the LABG, HAGB, and CTB samples, respectively. Defect quantification methodology is described in Supplemental Material (Figure S4). The defect density values for all three GBs showed an initial increase (but to different magnitudes) then modulated at different amplitudes. For the low angle sample, the defect density values had the most variance after irradiation going between $11 \cdot 10^{22}$ m^{-3} and $37 \cdot 10^{22}$ m^{-3}. The high angle defect density values wavered between $4 \cdot 10^{22}$ m^{-3} and $23 \cdot 10^{22}$ m^{-3}, and the Σ3 defect density climbed fairly consistently with values spanning from $4 \cdot 10^{22}$ m^{-3} to $18 \cdot 10^{22}$ m^{-3}. The defect absorption rates calculated from the linear trend-

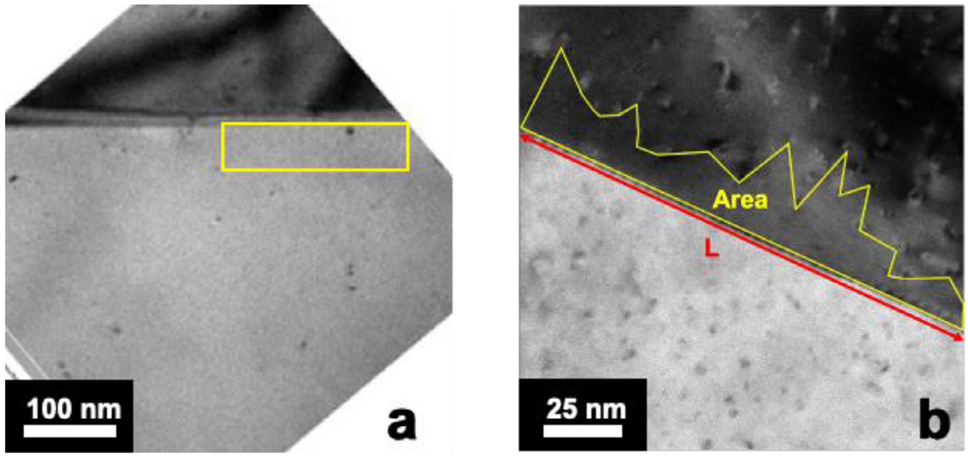

Fig. 2. Depiction of quantitative defect analysis: (a) still image extracted from in situ irradiation video of the LAGB; yellow box identifies 50 nm x 200 nm area in which defect density was calculated. (b) TEM image of LAGB annotated with parameters used to measure defect denuded zone width.

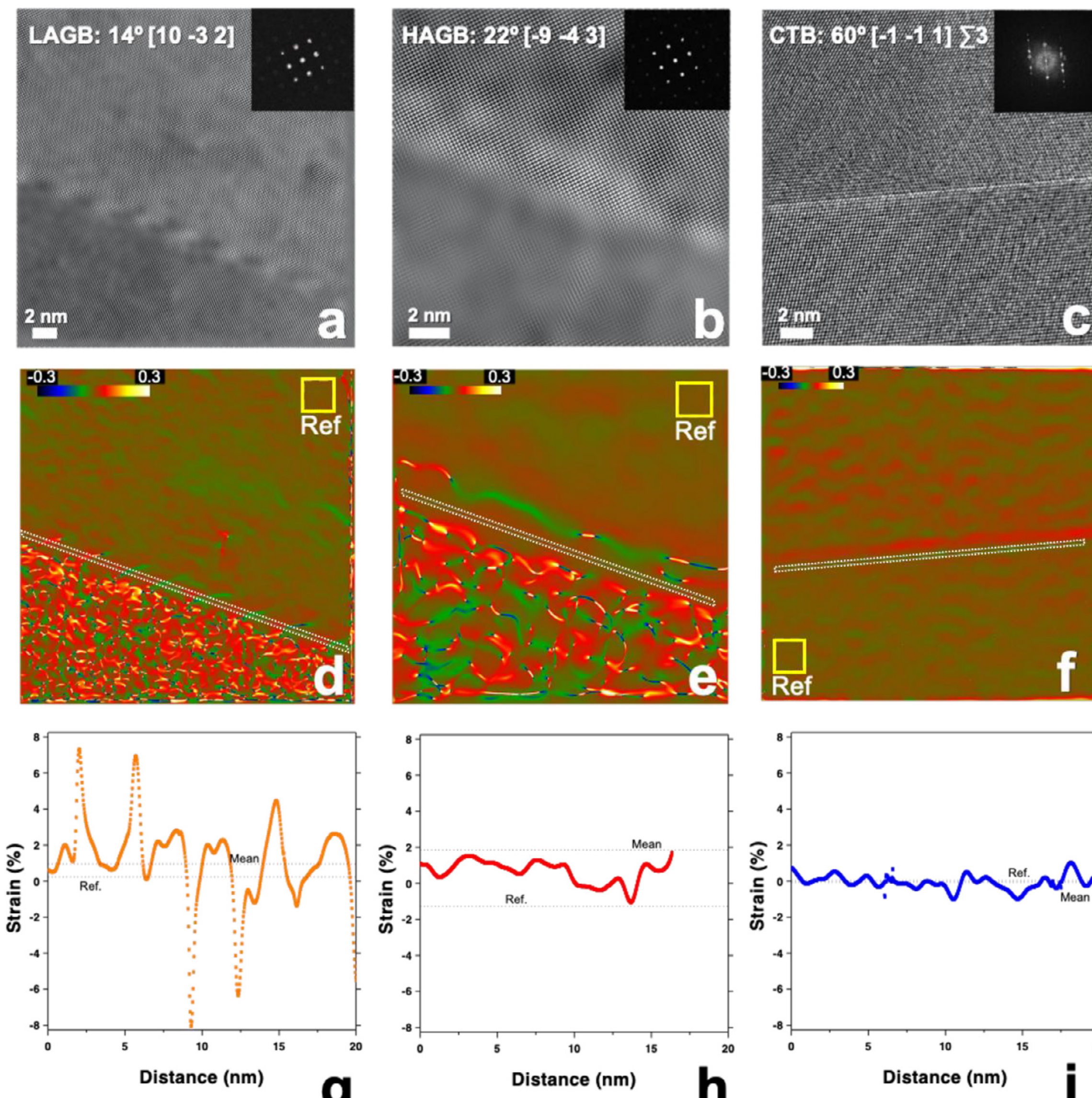

Fig. 3. Pre-irradiation high-resolution, bright field micrographs (with insets of Fourier transform) of (a) LAGB, (b) HAGB, and (c) CTB boundaries. Deformation maps corresponding to (d) LABG, (e) HAGB, and (f) CTB produced via GPA of the corresponding micrographs. Extracted strain (ε_{xy}) profile acquired from the ROI (identified by the dotted white outlined boxes) adjacent to the (g) LAGB, (h) HAGB, and (i) CTB.

Table 1
Interfacial strain and defect absorption rates at the GB.

GB Type	GB Misorientation	GB Plane	Interfacial Strain (%) - Mean	Interfacial Strain(%) - StdDev	Defect Absorption Rates (-10^{22} $m^{-3}s^{-1}$)
LAGB	14° [10 −3 2]	{−1 1 0}	0.71	2.41	0.20
HAGB	22° [−9 −4 3]	{1 1 0}	0.64	0.61	0.09
CTB	60° [−1 −1 1] Σ3	{1 1 1}	−0.07	0.39	0.01

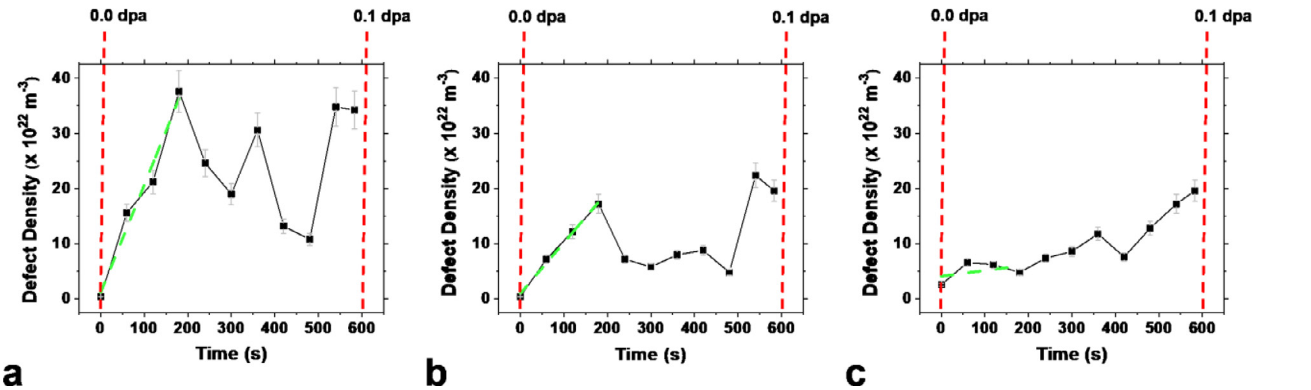

Fig. 4. Defect density as a function of time for the (a) LAGB (14º), (b) HAGB (22º) GB, and (c) CTB Σ3 (60º) GB; green dotted line represents the trendline from which the defect absorption rate was calculated. Error bars represent 10% spread around the data points.

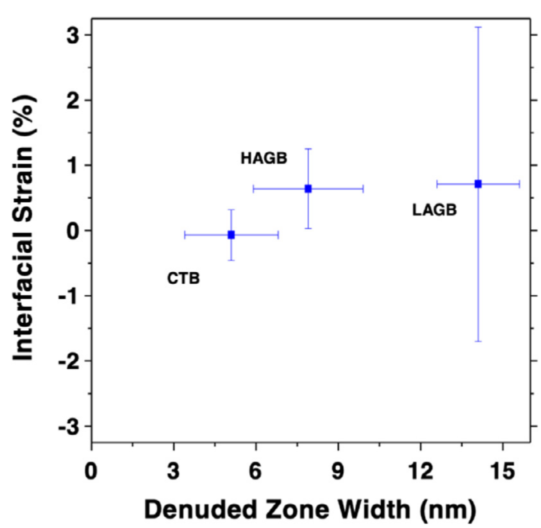

Fig. 5. Interfacial strain as a function of denuded zone width (and corresponding standard deviations) for the LAGB, HAGB, and coherent Σ3 GB.

lines were $0.20\cdot10^{22}$ $m^{-3}s^{-1}$, $0.09\cdot10^{22}$ $m^{-3}s^{-1}$, and $0.01\cdot10^{22}$ $m^{-3}s^{-1}$ for the low angle, high angle, and Σ3 GBs, respectively, and are listed in Table 1.

The calculated relative interfacial strain values measured for the three GBs in the pristine state are presented as a function of denuded zone widths in Fig. 5. The LAGB had the largest denuded zone at 14.1 ± 1.5 nm, followed by the HAGB at 7.9 ± 2.0 nm. The coherent Σ3 GB denuded zone was measured to be 5.1 ± 1.7 nm, which is less than the mean distance between defects in the adjacent grain, 12.7 ± 3.6 nm, as listed in Table S1. The observation that the defect denuded zone width is smaller than the mean distance between defects asserts the minimal effect of special boundaries on denuded zone widths, and suggests the absence of a definitive defect denuded zone. GB character in the LAGB and the HAGB demonstrates a discernible effect on denuded zone width, as the mean distance between defects in the grains adjacent to the LAGB and the HAGB were 6.5 ± 3.7 nm and 3.7 ± 2.5 nm, respectively. The LAGB had the largest denuded zone width, highest interfacial strain, and largest standard deviation for the strains measured compared to the other two GBs. It is interesting to note that upon visual inspection of the micrograph of the LAGB in Fig. 3, dislocation cores are clearly visible traversing the length of the GB and extending toward the grain lattice. The large changes, nearly 5% variance, in the strain values for the LAGB evidently correspond with the placement of the dislocation cores. The HAGB did not exhibit dislocation core structures along the GBs like the LAGB, nor did the coherent Σ3 GB, and the standard deviation of the measured strains were four times less than the LAGB.

4. Discussion

Observations pertaining to the HAGB and the CTB were consistent with previous works [9,18] where VDZ were minimal at special boundaries, such as the Σ3⟨1 1 0⟩ tilt GB, and increased with the GB plane inclination angle and for non-Σ3/random HAGBs; nevertheless, the most interesting result pertained to the LAGB. Contrary to instinctive predispositions of random HAGBs instituting the upper rate limit for defect absorption, a theoretical study by Szlufarska et al. [66] showed that the sink strength of low-angle GBs can exceed that of high-angle GBs due to the effect of GB stress fields. One might expect LAGBs to be poor sinks for point defects and clusters and that their presence would invariably exhibit a diminished ability to resist radiation damage compared to HAGBs due to tilt GBs with small misorientation angles (<15º) containing a lower dislocation density than GBs with larger angles (>15º); however, conversely the results from the study at hand support Szlufarska et al.'s claims with the 14º low-angle GB having the largest divergences in strain, highest defect absorption rate, and largest defect denuded zone width of the three GBs studied.

Szlufarska et al. calculated sink strength as a function of misorientation angle for both interstitials and vacancies in fcc Cu. The GB sink strength for interstitials exhibited a maximum at a misorientation angle of ~2º and decreased sharply as the angle approached 0º; interstitial sink strength also decreased and approached the value of a continuous planar sink as the misorientation angle increased. For vacancies above a misorientation angle of around 4º, the sink strength was constant, and the sink strength decreased when angle was less than 4º. The authors explained that vacancy-

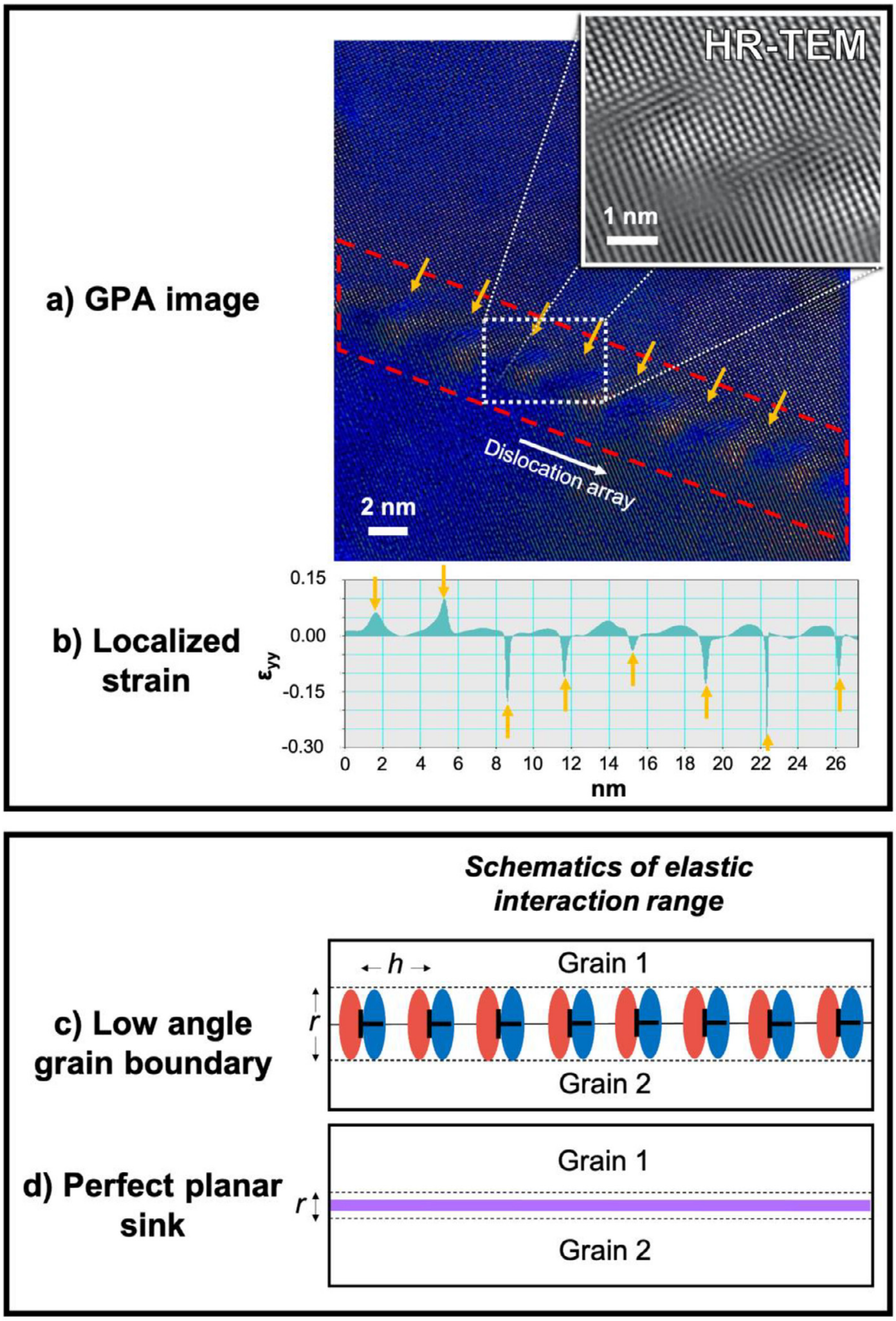

Fig. 6. Relationship between grain boundary strain and interaction range (a) Lattice rotation map generated via geometric phase analysis (GPA) of the high-resolution filtered micrograph of 14º LAGB shown in Fig. 3a.; inset of magnified image of dislocation core structure of the GB area annotated by the white dashed rectangle. (b) Plot of localized strain variation of GB area annotated by red dashed trapezoid in Fig. 6(a); yellow arrows indicate dislocation core spacings extending from GB. Schematic representations of a (c) LAGB and (d) a perfect planar sink, i.e. an idealized random HAGB, exhibiting the extent of the elastic interaction between defects and the GBs, where h is the dislocation separation distance and r is the characteristic length of elastic interaction field, i.e. the furthest distance away from GB plane where elastic interaction energy is equal to the thermal energy. On the LAGB, red and blue regions indicate positive and negative elastic interaction energy, respectively; opposite signs are above and below the dislocation glide plane. Contrarily, a perfect planar sink, formed when dislocation cores merge, is shrouded in purple indicating the cohesion of elastic interaction energy.

stress field interactions are much weaker in comparison, as interstitials have a relaxation volume six times that of a vacancy. The model predicted generally constant sink strength for vacancies consistent with existing experimental data where very little variation was measured for the denuded zones of GBs with misorientations $>\sim 2º$, except in the case of special coherent $\Sigma 3$ twin boundaries [67–69].

We assert that the higher defect absorption rate for the LAGB is consequent of higher strain magnitude effectively attracting more point defects compared to the HAGB and the CTB. Fig. 6 depicts the relationship between interfacial strain and defect interaction. Referencing the lattice rotation map shown in Fig. 6a (corresponding to the LAGB depicted in the high-resolution micrograph and relative strain map in Fig 3a and d), dislocation core structures are clearly visible along the GB (see Fig. 6a inset). While local strain fields extending from each dislocation do not produce long range effects, presumably the hydrostatic components of the stress imposed interacts with the volumetric strain of point defects in the vicinity of the GB produced in the damage cascades. This phenomenon is not present in HAGBs because as tilt angles exceed

15º, dislocations begin to overlap, hence historically, HAGBs have been modeled as continuous planar sinks. A LAGB can be modeled as a partition composed of parallel edge dislocations as depicted schematically in Fig. 6c; the stress field of a low-angle symmetric tilt GB can be calculated by superimposing the stress fields of an array of parallel dislocations and is composed of both normal and shear components. It has been expressed analytically and via molecular dynamics (represented schematically in Fig. 6d) that generally as GB misorientation angles increase, stress decreases, i.e. for HAGBs, dislocation density increases causing their local stress fields to cancel as GB angle increases, ultimately resulting in sink strength decreasing [66,70].

Twin GBs have been well studied and it is generally accepted that coherent $\Sigma3$ GBs are very stable and have little interaction with defects compared to random grain boundaries [16,18]. Moreover, in the current study, the $\Sigma3$ GB having the lowest strain and slowest defect absorption rate was anticipated. The fairly steady increasing defect density in the $\Sigma3$ sample is characteristic of the GB having minimal interaction with irradiation-induced defects, not being an effective sink, and the defects consistently building up with continued bombardment. On the contrary, the defect densities for the low-angle and high-angle GBs exhibit incessant fluctuations which can be interpreted as side effect of defects congregating, arranging, and being absorbed. We assert that the variability of the HAGB and LAGB's defect densities with sustained irradiation correspond to defect absorption, accommodation, and the subsequent structural modifications, which in turn instigate changes in sink efficiency comparable to the phenomena described by Bai et al. and Frolov et al. [27,29,30]. Results from a phase field model of dislocation climb describing defect absorption at LAGBs show that GB sink strength is not only determined by long-range defect diffusions (such as in the case of a perfect sink) but also the short-range reactions between defects and dislocations such as in the mechanisms related to vacancy absorption at dislocation jogs [71]. In a model study in Cu, Uberuaga et al. [31] found that damaged GBs, modeled as boundaries with excess defect content, would have stronger interactions with defects in the bulk of the material differing dramatically from pristine GBs. This led them to resolve that the sink efficiencies of interfaces are not static quantities but evolve in a complex manner during irradiation, as the concentration of defects within the GB will depend on both boundary structure and irradiation conditions. These recent findings advocating how structural adaptation and multiplicity affects the mechanisms of the defect absorption explain the fluctuations in defect densities and effectively perturbed absorption rates.

In transparency, we recognize that "absorption rate" is a loaded term that embeds the possibility of adjacent recombination/annihilation events, and that those events could be locally enhanced or exacerbated by intrinsic and extrinsic dislocations in the GB. Intrinsic dislocations are present in the LAGB equilibrium structure prior to irradiation, resultant from the misfit of two lattices, inducing periodic arrays of dislocations, or dislocation cores [72]. The LAGB exhibits more strain due to the extending dislocation cores hence more defects are attracted and congregate at the interface; however, though the LAGB may demonstrate stronger defect attraction and accumulation at the interface, subsequent annihilation rather than full absorption may occur. Chen et al. [73] recently established that capability of a GB to absorb Frank loops is dependent on the misorientation angle and local structural units. Theoretically, a LAGB will have less free volume compared to a HAGB, therefore, there will be less space for the defects to be accommodated. In Szlufarska et al.'s model, the implicit Crank–Nicolson scheme is incorporated to account for sink strength being time-dependent. For both vacancy and an interstitial sink strength as a function of time, it was determined that the GB sink strength is initially very high (infinite at $t = 0$ s) then approaches steady-state values beyond 1.0 nanoseconds. Since the diffusivity of interstitials is orders of magnitude faster than that of vacancies, the steady state is reached much faster for interstitials than for vacancies (>2 s). For LAGBs, in particular, the time-dependent sink strength of interstitials was consistently larger than that of the perfect planar sink (i.e., a HAGB), whereas the vacancy sink strength was very similar to that of the perfect planar sink. This is credited to the relaxation volume of the interstitial being 22.44 Å^3 compared to -3.80 Å^3 for vacancies. These conclusions are also in line with the absorption rate data as interstitials insistently seek the free volume within the dislocation cores in the LAGB. The model competently describes the defect-sink relation but only up to a certain point; with increasing time, the concentration of point defects approaches the steady-state solution in which the GB is saturated, however this does not account for structural reorganization or transformations as prescribed by Bai et al. and Frolov et al. Structural reconfigurations potentially allow for a sink strength "reset" without altering the GB macroscopic character while permitting the interface to continue accommodating more defects. Foley and Tucker [13] contend that under continuous damage accumulation, a grain boundary will evolve through many non-equilibrium states until a steady "damaged" state is found that is higher in both energy and free volume than the equilibrium state. The erraticism (or the stability in the case of the CTB) of the defect densities is perceived as an artifact of defect coaction amid the respective free volume in the GBs. It is also of interest to note Frolov et al.'s [30] detection of the temperature dependence of GB free volume and structure, furthermore, accentuating how sink efficiency is effected in addition to diffusion parameters.

The affinities between interfacial strain and sink strength are spatially articulated in Fig. 5. The dislocation cores extending from the LAGB strongly affect defect absorption, compared to the HAGB and CTB, as evidenced by the significant denuded zone width underlining a localized factor to defect-sink interactions. Comparably, experimental results suggest that non-equilibrium GBs may have higher sink strengths than their equilibrium counterparts and provide ample radiation toleration [6,74,75]. Non-equilibrium GBs characteristically possess excess defect concentrations, disordered regions, steps, ledges, extrinsic defects, and more complex dislocation/disclination systems; these features correlate to relatively higher energy, strain, excess free volume, disordered atomic structure, and energetically metastable states compared to their equilibrium analogs. Simulations have shown that the excess free volume contained by non-equilibrium GBs contribute to a decreased survival rate of point defects produced in damage cascades in the vicinity of the GB [76]. In an in situ irradiation experiment, Vetterick et al. found that nanocrystalline Fe comprised of non-equilibrium GBs contained both a lower number density of defect clusters and a smaller average defect cluster size compared to an annealed, thermodynamically stabilized sample with equilibrium GBs irradiated under the same conditions [77]. Similar to the distinguishable dislocations of the LAGB, stair configuration structural units have been identified in twin GBs to accommodate misfits within 10° deviated from the perfect structure [78–81]. The resolved stress associated with the complex, local dislocation content of LAGBs, deviated special boundaries, and non-equilibrium GBs manifest greater excess free volume compared to random HAGBs; however, it remains to be systematically studied if these aberrant interfaces encourage extensive defect-GB interactions that may potentially enhance sink efficiency and radiation tolerance.

5. Conclusion

The results from this work provide definitive evidence of interfaces differing in macroscopic character displaying unique defect absorption proclivities. The study resolved defect sink efficiency as a function of interfacial strain associated with GB character, and furthermore, showing that the proficiency for GBs to absorb defects is not necessarily static and can exhibit substantial variability even at low irradiation doses. Interestingly, the LAGB (14º misorientation) possessed the largest relative strain and exhibited the fastest defect absorption rate and widest defect denuded zone, compared to a random HAGB (22º misorientation) and a coherent $\Sigma 3$ GB. The research combined quantitative microstructure analysis at high-resolution with defect absorption rate and denuded zone measurements. The discernable dislocation content of the LAGB manifested localized strain gradients which encouraged extensive GB-defect interactions enhancing sink efficiency.

These experimental results corroborate literature reporting microscopic degrees of freedom crystallographic parameters – not just GB plane and misorientation angle – and also play an important role in determining the sink efficiencies of GBs. This work provides the first systematically acquired quantitative experimental evidence supporting the GB strain-interstitial accommodation model presented by Samaras et al. [43] and Szlufarska et al.'s [66] conjecture that LAGBs can be more efficient defect sinks compared to HAGBs. Though relations detailing the structure of distinctive GBs with atypical features (i.e. protruding dislocations, stair configurations, excessive extrinsic dislocation content) and their effect on absorption are currently not available, The development of a model to describe absorption events in the instance of dislocation cores and variance in local strain may markedly propel efforts at designing advanced, more radiation tolerant materials via GB engineering. Furthermore, more systematic studies of local features such as GB structural units are required to understand interface-defect interactions and absorption regarding GB character and metastability.

Declaration of Competing Interest

The authors declare that they have no known competing financial interests or personal relationships that could have appeared to influence the work reported in this paper.

Acknowledgments

M.L.T., E.M.H. and J.E.N. acknowledge funding from the U.S. Department of Energy, Office of Basic Energy Sciences, through contract DE-SC0020314, and in part under grant DE-SC0008274 (M.L.T. and P.K.S.). Use of the Center for Nanoscale Materials, an Office of Science user facility, was supported by the U.S. Department of Energy, Office of Science, Office of Basic Energy Sciences, under Contract No. DE-AC02-06CH11357. Authors acknowledge Dr. Chang-Yu Hung of Johns Hopkins University for helpful discussions.

Supplementary materials

Supplementary material associated with this article can be found, in the online version, at doi:10.1016/j.actamat.2022.117624.

References

[1] N.V. Doan, G. Martin, Elimination of irradiation point defects in crystalline solids: sink strengths, Phys. Rev. B 67 (2003) 1–11, doi:10.1103/PhysRevB.67.134107.
[2] A.H. King, D.A. Smith, On the mechanisms of point-defect absorption by grain and twin boundaries, Philoso. Mag. A 42 (1980) 495.
[3] R.C. Pond, D.A. Smith, On the absorption of dislocations by grain boundaries, Philoso. Mag. 36 (1977) 353–366, doi:10.1080/14786437708244939.
[4] I.J. Beyerlein, M.J. Demkowicz, A. Misra, B.P. Uberuaga, Defect-interface interactions, Prog. Mater Sci. 74 (2015) 125–210, doi:10.1016/j.pmatsci.2015.02.001.
[5] J. Han, S.L. Thomas, D.J. Srolovitz, Grain-boundary kinetics : a unified approach, Prog. Mater Sci. 98 (2018) 386–476, doi:10.1016/j.pmatsci.2018.05.004.
[6] X. Zhang, K. Hattar, Y. Chen, L. Shao, J. Li, C. Sun, K. Yu, N. Li, M.L. Taheri, H. Wang, J. Wang, M. Nastasi, Radiation damage in nanostructured materials, Prog. Mater Sci. 96 (2018) 217–321, doi:10.1016/j.pmatsci.2018.03.002.
[7] K.G. Field, Y. Yang, R. Allen, J.T. Busby, Defect sink characteristics of specific grain boundary types in 304 stainless steels under high dose neutron environments, Acta Mater. 89 (2015) 438–449, doi:10.1016/j.actamat.2015.01.064.
[8] L.K. Mansur, A.D. Brailsford, W.G. Wolfer, On the meaning of sink capture efficiency and sink strength for point defects, J. Nucl. Mater. 105 (1982) 36–38, doi:10.1016/0022-3115(82)90449-4.
[9] W.Z. Han, M.J. Demkowicz, E.G. Fu, Y.Q. Wang, A. Misra, Effect of grain boundary character on sink efficiency, Acta Mater. 60 (2012) 6341–6351, doi:10.1016/j.actamat.2012.08.009.
[10] H. Gleiter, Grain boundaries as point defect sources or sinks—Diffusional creep, Acta Metall. 27 (1979) 187–192, doi:10.1016/0001-6160(79)90095-6.
[11] M. Rose, A.G. Balogh, H. Hahn, Instability of irradiation induced defects in nanostructured materials, in: Nuclear Instruments and Methods in Physics Research Section B: Beam Interactions With Materials and Atoms. 127–128, 1997, pp. 119–122, doi:10.1016/S0168-583X(96)00863-4.
[12] S. Mao, S. Shu, J. Zhou, R.S. Averback, S.J. Dillon, Quantitative comparison of sink efficiency of Cu–Nb, Cu–V and Cu–Ni interfaces for point defects, Acta Mater. 82 (2015) 328–335, doi:10.1016/j.actamat.2014.09.011.
[13] D. Foley, J.D. Tucker, Quantifying grain boundary damage tolerance with atomistic simulations, Model. Simul. Mater. Sci. Eng. 24 (2016) 075011.
[14] O. El-Atwani, J.E. Nathaniel, A.C. Leff, K. Hattar, M.L. Taheri, Direct observation of sink-dependent defect evolution in nanocrystalline iron under irradiation, Sci. Rep. 7 (2017) 1836, doi:10.1038/s41598-017-01744-x.
[15] I.J. Beyerlein, M.J. Demkowicz, A. Misra, B.P. Uberuaga, Defect-interface interactions, Prog. Mater Sci. 74 (2015) 125–210, doi:10.1016/j.pmatsci.2015.02.001.
[16] W. Han, E.G. Fu, M.J. Demkowicz, Y. Wang, A. Misra, Irradiation damage of single crystal, coarse-grained, and nanograined copper under helium bombardment at 450 °c, J. Mater. Res. 28 (2013) 2763–2770, doi:10.1557/jmr.2013.283.
[17] Y. Chimi, A. Iwase, N. Ishikawa, M. Kobiyama, T. Inami, T. Kambara, S. Okuda, Swift heavy ion irradiation effects in nanocrystalline gold, Nucl. Instrum. Method. Phys. Res. Sect. B 245 (2006) 171–175, doi:10.1016/J.NIMB.2005.11.096.
[18] C.M. Barr, L. Barnard, J.E. Nathaniel, K. Hattar, K.A. Unocic, I. Szlurfarska, D. Morgan, M.L. Taheri, Grain boundary character dependence of radiation-induced segregation in a model Ni-Cr alloy, J. Mater. Res. 30 (2015) 1290–1299, doi:10.1557/jmr.2015.34.
[19] W. Liu, Y. Ji, P. Tan, H. Zang, C. He, D. Yun, C. Zhang, Z. Yang, Irradiation induced microstructure evolution in nanostructured materials: a review, Materials (Basel) 9 (2016) 1–15, doi:10.3390/ma9020105.
[20] M.A. Tschopp, D.L. McDowell, Atomistic simulations of dislocation nucleation in single crystals and grain boundaries, Philos. Mag. 87 (2007) 3147.
[21] O. El-Atwani, J.E. Nathaniel, A.C. Leff, J.K. Baldwin, K. Hattar, M.L. Taheri, Evidence of a temperature transition for denuded zone formation in nanocrystalline Fe under He irradiation, Mater. Res. Lett. 5 (2017) 195–200, doi:10.1080/21663831.2016.1243591.
[22] C.M. Barr, O. El-atwani, D. Kaoumi, K. Hattar, Interplay between grain boundaries and radiation damage, JOM 71 (2019) 1233–1244, doi:10.1007/s11837-019-03386-y.
[23] Y. Sekio, N. Sakaguchi, Effect of nickel concentration on radiation-induced diffusion of point defects in high-nickel Fe--Cr-Ni model alloys during neutron and electron irradiation, Mater. Trans. 60 (2019) 678–687.
[24] X. Bai, L.J. Vernon, R.G. Hoagland, A.F. Voter, M. Nastasi, B.P. Uberuaga, Role of atomic structure on grain boundary-defect interactions in Cu, Phys. Rev. B 214103 (2012) 1–10, doi:10.1103/PhysRevB.85.214103.
[25] W.S. Yu, M.J. Demkowicz, Non-coherent Cu grain boundaries driven by continuous vacancy loading, J. Mater. Sci. 50 (2015) 4047, doi:10.1007/s10853-015-8961-9.
[26] O. El-Atwani, J.E.E. Nathaniel, A.C.C. Leff, K. Hattar, M.L.L. Taheri, Direct observation of sink-dependent defect evolution in nanocrystalline iron under irradiation, Sci. Rep. 7 (2017) 1–12, doi:10.1038/s41598-017-01744.
[27] X.M. Bai, A.F. Voter, R.G. Hoagland, M. Nastasi, B.P. Uberuaga, Efficient annealing of radiation damage near grain boundaries via interstitial emission, Science 327 (2010) 1631–1634, doi:10.1126/science.1183723.
[28] G. Ackland, Controlling radiation damage, Science 327 (2010) 1587–1588.
[29] T. Frolov, S.V. Divinski, M. Asta, Y. Mishin, Effect of interface phase transformations on diffusion and segregation in high-angle grain boundaries, Phys. Rev. Lett. 110 (2013) 255502.
[30] T. Frolov, D.L. Olmsted, M. Asta, Y. Mishin, Structural phase transformations in metallic grain boundaries, Nat. Commun. 4 (2013) 1899.
[31] B.P. Uberuaga, L.J. Vernon, E. Martinez, A.F. Voter, The relationship between grain boundary structure, defect mobility, and grain boundary sink efficiency, Sci. Rep. 9095 (2015) 1–9, doi:10.1038/srep09095.
[32] P.C. MILLETT, D.S. AIDHY, T. DESAI, S.R. PHILLPOT, D. WOLF, Grain-boundary source/sink behavior for point defects : an atomistic simulation study, Int. J. Mater. Res. 100 (2009) 550–555 NP–6.
[33] G.S. Was, Fundamentals of Radiation Materials Science, 2007, doi:10.1007/978-3-540-49472-0.
[34] A.D. Brailsford, R. Bullough, The Theory of Sink Strengths, Philoso. Trans. Roy. Soc. Lond. 302 (1981) 87–137.
[35] R.W. Balluffi, A.V. Granato, Dislocations in Solids, 1979 North-Holland, New York.
[36] M.J. Demkowicz, R.G. Hoagland, B.P. Uberuaga, A. Misra, Influence of interface sink strength on the reduction of radiation-induced defect concentrations and fluxes in materials with large interface area per unit volume, Phys. Rev. B 84 (2011) 1–5, doi:10.1103/PhysRevB.84.104102.
[37] R.W. Balluffi, T. Kwok, P.D. Bristowe, A. Brokman, P.S. Ho, S. Yip, Determination of vacancy mechanism for grain boundary self- diffusion by computer simulation, Scr. Metall. 15 (1981) 951.

[38] T. Kwok, P.S. Ho, S. Yip, R.W. Balluffi, P.D. Bristowe, A. Brokman, Evidence for vacancy mechanism in grain boundary diffusion in bcc iron: a molecular-dynamics study, Phys. Rev. Lett. 47 (1981) 1148.
[39] M. Sorensen, Y. Mishin, A. Voter, Diffusion mechanisms in Cu grain boundaries, Phys. Rev. B 62 (2000) 3658–3673.
[40] I.J. Beyerlein, A. Caro, M.J. Demkowicz, N.A. Mara, A. Misra, B.P. Uberuaga, Radiation damage tolerant nanomaterials, Mater. Today 16 (2013) 443–449, doi:10.1016/j.mattod.2013.10.019.
[41] D. Bamney, L. Capolungo, D.E. Spearot, Role of equilibrium and non-equilibrium grain boundary stress fields on dislocation transmission, J. Mater. Res. (2021), doi:10.1557/s43578-021-00129-1.
[42] M. Samaras, P.M. Derlet, H. Van Swygenhoven, M. Victoria, H. Van Swygenhoven, M. Victoria, Computer Simulation of Displacement Cascades in Nanocrystalline Ni, Phys. Rev. Lett. 88 (2002) 125505, doi:10.1103/PhysRevLett.88.125505.
[43] M. Samaras, P.M. Derlet, H. Van Swygenhoven, M. Victoria, SIA activity during irradiation of nanocrystalline Ni, J. Nucl. Mater. 323 (2003) 213–219, doi:10.1016/j.jnucmat.2003.08.020.
[44] K. Inderjeet, Y. Mishin, W. Gust, Fundamentals of Grain and Interphase Boundary Diffusion, John Wiley, Chichester, 1995.
[45] G. Gottstein, L.S. Shvindlerman, Grain Boundary Migration in metals: thermodynamics, kinetics, Applications, CRC press, 2009.
[46] T. Watanabe, S.-I. Kimura, S. Karashima, The effect of a grain boundary structural transformation on sliding in <1010>-tilt zinc bicrystals, Philos. Mag. A 49 (1984) 845–864, doi:10.1080/01418618408236566.
[47] M.J. Hytch, E. Snoeck, R. Kilaas, Quantitative measurement of displacement and strain fields from HREM micrographs, Ultramicroscopy 74 (1998) 131–146.
[48] M.J. Hytch, J.-L. Putaux, J. Thibault, Stress and strain around grain-boundary dislocations measured by high-resolution electron microscopy, Philos. Mag. 86 (2006) 4641–4656, doi:10.1080/14786430600743876.
[49] P. Taylor, M. Sennour, Y. Champion, M.J. Hÿtch, HRTEM study of defects in twin boundaries of ultra-fine grained copper, Philos. Mag. 87 (2007) 1465–1486, doi:10.1080/14786430601021611.
[50] C.L. Johnson, E. Snoeck, M. Ezcurdia, B.R.I. Alez, I. Pastoriza-santos, L.M.L. An, Effects of elastic anisotropy on strain distributions in decahedral gold nanoparticles, Nat. Mater. 7 (2008), doi:10.1038/nmat2083.
[51] H. Rösner, C.T. Koch, G. Wilde, Strain mapping along Al-Pb interfaces, Acta Mater. 58 (2010) 162–172, doi:10.1016/j.actamat.2009.08.065.
[52] H. Rösner, N. Boucharat, K.A. Padmanabhan, J. Markmann, G. Wilde, Strain mapping in a deformation-twinned nanocrystalline Pd grain, Acta Mater. 58 (2010) 2610–2620, doi:10.1016/j.actamat.2009.12.047.
[53] C.M. Barr, G.A. Vetterick, K.A. Unocic, K. Hattar, X.-M. Bai, M.L. Taheri, Anisotropic radiation-induced segregation in 316 L austenitic stainless steel with grain boundary character, Acta Mater. 67 (2014) 145–155, doi:10.1016/j.actamat.2013.11.060.
[54] J.L. Rouvière, A. Mouti, P. Stadelmann, Measuring strain on HR-STEM images : application Measuring strain on HR-STEM images : application to, J. Phys. Conf. Ser. 326 (2011) 012022, doi:10.1088/1742-6596/326/1/012022.
[55] D. Cooper, T. Denneulin, N. Bernier, A. Béché, J.L. Rouvière, Strain mapping of semiconductor specimens with nm-scale resolution in a transmission electron microscope, Micron 80 (2016) 145–165, doi:10.1016/j.micron.2015.09.001.
[56] M. Haider, S. Uhlemann, E. Schwan, H. Rose, B. Kabius, K. Urban, Electron microscopy image enhanced, Nature 392 (1998) 768–769, doi:10.1038/33823.
[57] K.W. Urban, Studying atomic structures by aberration-corrected transmission electron microscopy, Science 321 (2008) 506–511.
[58] M.J. Hytch, P. Bayle, in: Proc. 13th International Congress on Electron Microscopy (ICEM 13), in: Editions de Physique, Paris, 1994, p. 129.
[59] M.J. Hytch, M. Gandais, Quantitative criteria for the detection and characterization of nanocrystals from high-resolution electron microscopy images, Philos. Mag. A 72 (1995) 619–634.
[60] J.-.P. Deville, M. Hanbücken, Stress and Strain in Epitaxy: Theoretical Concepts, Measurements and Applications, Elsevier, 2001.
[61] J.L. Taraci, M.J. Hÿtch, T. Clement, P. Peralta, M.R. McCartney, J. Drucker, S.T. Picraux, Strain mapping in nanowires, Nanotechnology 16 (2005) 2365–2371, doi:10.1088/0957-4484/16/10/062.
[62] N. Cherkashin, M.J. Hÿtch, E. Snoeck, A. Claverie, J.M. Hartmann, Y. Bogumilowicz, Quantitative strain and stress measurements in Ge/Si dual channels grown on a Si0. 5Ge0. 5 virtual substrate, Mater. Sci. Eng. 124 (2005) 118–122.
[63] M.J. Hÿtch, F. Houdellier, Mapping stress and strain in nanostructures by high-resolution transmission electron microscopy, Microelectron. Eng. 84 (2007) 460–463, doi:10.1016/j.mee.2006.10.062.
[64] M.J. Hÿtch, J.-.L. Putaux, J.-.M. Pénisson, Measurement of the displacement field of dislocations to 0.03 Å by electron microscopy, Nature 423 (2003) 270–273, doi:10.1038/nature01638.
[65] J.E. Nathaniel, A.C. Lang, O. El-atwani, P.K. Suri, J.K. Baldwin, M.A. Kirk, Y. Wang, M.L. Taheri, Toward high-throughput defect density quanti fi cation : a comparison of techniques for irradiated samples, Ultramicroscopy 206 (2019) 112820, doi:10.1016/j.ultramic.2019.112820.
[66] C. Jiang, N. Swaminathan, J. Deng, D. Morgan, I. Szlurfarska, Effect of grain boundary stresses on sink strength, Mater. Res. Lett. (2014) 3831, doi:10.1080/21663831.2013.871588.
[67] B.N. Singh, A.J.E. Foreman, Calculated grain size-dependent vacancy supersaturation and its effect on void formation, Philoso. Mag 29 (1974) 847–858, doi:10.1080/14786437408222075.
[68] B.K. Basu, C. Elbaum, Surface vacancy pits and vacancy diffusion in aluminum, Acta Metall. 13 (1965) 1117–1122, doi:10.1016/0001-6160(65)90048-9.
[69] R.W. Siegel, S.M. Chang, R.W. Balluffi, Vacancy loss at grain boundaries in quenched polycrystalline gold, Acta Metall. 28 (1980) 249–257, doi:10.1016/0001-6160(80)90159-5.
[70] J. Hirth, J. Lothe, Theory of Dislocations, Columbus, 1968.
[71] P. Liu, S. Zheng, K. Chen, X. Wang, B. Yan, P. Zhang, S. Shi, Point defect sink strength of low-angle tilt grain boundaries: a phase field dislocation climb model, Int. J. Plast. 119 (2019) 188–199, doi:10.1016/j.ijplas.2019.03.008.
[72] M. Dupeux, Extrinsic and intrinsic boundary dislocations, Philos. Mag. Lett. 55 (1987) 7–13, doi:10.1080/09500838708210433.
[73] J. Chen, K. Dang, H.T. Vo, P. Hosemann, S.J. Fensin, Associating GB characteristics with its sink efficiency in absorbing Frank loops in Cu, Scr. Mater. 192 (2021) 61–66, doi:10.1016/j.scriptamat.2020.10.006.
[74] X. Sauvage, G. Wilde, S. Divinsky, Z. Horita, R.Z. Valiev, Grain boundaries in ultrafine grained materials processed by severe plastic deformation and related phenomena, Mater. Sci. Eng. A 540 (2012) 1–12.
[75] M. Wurmshuber, D. Frazer, A. Bachmaier, Y. Wang, P. Hosemann, D. Kiener, Impact of interfaces on the radiation response and underlying defect recovery mechanisms in nanostructured Cu-Fe-Ag, Mater. Des. 160 (2018) 1148–1157, doi:10.1016/j.matdes.2018.11.007.
[76] M. Samaras, P.M. Derlet, H. Van Swygenhoven, M. Victoria, Radiation damage near grain boundaries, Philos. Mag. 83 (2003) 3599–3607, doi:10.1080/14786430310001600222.
[77] G.A. Vetterick, J. Gruber, P.K. Suri, J.K. Baldwin, M.A. Kirk, P. Baldo, Y.Q. Wang, A. Misra, G.J. Tucker, M.L. Taheri, Achieving radiation tolerance through non-equilibrium grain boundary structures /639/301/357/537 /639/301/1023 article, Sci. Rep. 7 (2017) 1–9, doi:10.1038/s41598-017-12407-2.
[78] J.P. Hirth, R.C. Pond, Steps, dislocations and disconnections as interface defects relating to structure and phase transformations, Acta Mater. 44 (1996) 4749–4763, doi:10.1016/S1359-6454(96)00132-2.
[79] J.P. Hirth, R.C. Pond, J. Lothe, Disconnections in tilt walls, Acta Mater. 54 (2006) 4237–4245, doi:10.1016/j.actamat.2006.05.017.
[80] M.A. Tschopp, G.J. Tucker, D.L. McDowell, Structure and free volume of< 1 1 0>symmetric tilt grain boundaries with the E structural unit, Acta Mater. 55 (2007) 3959–3969.
[81] M.A. Tschopp, G.J. Tucker, D.L. McDowell, Atomistic simulations of tension—compression asymmetry in dislocation nucleation for copper grain boundaries, Comput. Mater. Sci. 44 (2008) 351–362.